Interlayer exchange coupling and magnetoresistance in FM/Os/FM trilayers

2007 J. Phys.: Condens. Matter 19 386229

(http://iopscience.iop.org/0953-8984/19/38/386229)

IOP PUBLISHING JOURNAL OF PHYSICS: CONDENSED MATTER

J. Phys.: Condens. Matter **19** (2007) 386229 (14pp) doi:10.1088/0953-8984/19/38/386229

Interlayer exchange coupling and magnetoresistance in FM/Os/FM trilayers

K Zanat and A Boufelfel[1]

Physics Laboratory at Guelma, University of Guelma, PO Box 401, Guelma 24000, Algeria

E-mail: ahboufelfel@gmail.com

Received 30 July 2007, in final form 9 August 2007
Published 4 September 2007
Online at stacks.iop.org/JPhysCM/19/386229

Abstract

We have performed self-consistent calculations to study the interlayer exchange coupling and transport properties of FM/Os/FM trilayers (FM = Co, Fe, FeCo and FePt) as a function of the osmium spacer thickness. Our results are in a good agreement with the published experimental results. The antiferromagnetic (AF) coupling observed experimentally in trilayers where Os spacer thickness was 9–10 Å and where the ferromagnetic slabs were Fe, Co and FeCo verify very well our calculated results. For FePt/Os/FePt, we have attributed the AF coupling peak observed experimentally at a one monolayer (1 ML) Os spacer thickness to our calculated AF coupling at 1 ML in a disordered magnetic layer and, by introducing the effect of the interface roughness in our calculations, we found that the peak is shifted towards 1.5 ML. We fitted our interlayer exchange coupling (IEC) results to an Ruderman–Kittel–Kasuya–Yosida (RKKY) function to the third order to obtain the periods of oscillations and their strengths quantitatively. We have found in a Co/Os/Co trilayer that the values of the oscillation periods of the IEC are 4 and 7 ML; the latter was observed experimentally. Due to the lack of experimental data for the periods of oscillations in FeCo/Os/FeCo, Fe/Os/Fe and FePt/Os/FePt, we compared our results to another method of calculation and found good agreement. An enhancement in the giant magnetoresistance (GMR) is observed for an ordered ferromagnetic slab compared to systems with a disordered ferromagnetic slab.

1. Introduction

Artificial, man-made magnetic metallic multilayers have fascinated a great deal of experimental and theoretical researchers for more than the last two decades [1, 2]. One of the driving forces for these investigations is the potential application of such multilayers for data storage and spin-dependent transistors.

[1] Author to whom any correspondence should be addressed.

One family of these multilayers is formed by ferromagnetic layers and spacers of various material properties with a thickness of only a few atomic layers, and these have revealed phenomena which simply do not exist in other materials known to man so far. For the case of a metallic spacer, the interlayer exchange coupling (IEC) phenomenon was observed [3], which is based on the transfer of electron spins from one ferromagnetic film into another across a non-ferromagnetic spacer, as well as giant magnetoresistance (GMR), which is a consequence of the scattering of the spin at the interfaces. Two other discovered processes which are not discussed in this paper are: tunneling magnetoresistance (TMR) and the spin-transfer torque effect [4].

Regarding our interest in this paper, osmium (Os) based magnetic multilayered structures, where Os is the non-magnetic slab, have been studied experimentally [5–8] and theoretically [9]. It is known that Os has very high melting and boiling points, which are predicted to have a good effect on preventing interdiffusion between layers induced by agitation processes present in annealing or deposition techniques. Peng *et al* studied the thermal stability of FeCo/OsMn [10] and FeCo/IrMn [11] multilayers as function of annealing temperature and the thickness of a thin layer of Os inserted at the interface. They found that the interface of FeCo/OsMn shows better thermal stability after 400 °C annealing, despite the fact that the Os thickness was as thin as 3 Å. Furthermore, with a 3 Å Os barrier, the 350 °C annealed CoFe/Os/IrMn/CoFe showed the same magnetic behavior as the as-deposited state. Owing to this property of Os, theoretical calculations where sharp interfaces were assumed could be compared with experimental results.

It has been shown that the measured oscillation period of IEC in a Co/Os multilayer was 15 Å [5], which is unique in 3d, 4d and 5d transition metals, where the general trend for oscillation periods is in the range 9–12 Å [12, 13]. On the same footing, the 18 Å oscillation period of chromium is another exception [14–16].

Ru-based spacer layers have been studied extensively both experimentally and theoretically. Ironically, the experimental results were very controversial. As a matter of fact, the only theoretical calculations that agreed with part of the experimental findings are those of Stoeffler *et al* [17, 18] to our knowledge. Despite the fact that Ru and Os have the same phase and very close cell parameters, very little experimental work could be found in the literature for Os-based spacer layers.

The aim of this study is to investigate the oscillation of the interlayer exchange coupling versus the Os spacer thickness and its consequences on the magnetoresistance using self-consistent *ab initio* calculations. A comparison with recent experimental data is given.

2. Methodology

The surface Green function (SGF) is one of the powerful techniques that are used to study the magnetic and transport properties of trilayer systems [19, 20]. Based on two-dimensional periodicity, the SGF technique guarantees a physically correct description of a system consisting of a substrate and a magnetic trilayer where in the other methods, based on three-dimensional translational periodicity, the Fermi energy changes by changing the thickness of the system, causing incompatibilities with respect to the magnetic slabs. Such a technique was used to study the effect of alloying in the magnetic and spacer layers, interdiffusion at the interface [21, 22] and disorder on the magnetic and transport properties in terms of the coherent potential approximation (CPA) [23, 24].

All results reported in this paper were obtained using an all-electron scalar relativistic version of the surface Green's function technique implemented within the framework of a tight binding linear muffin-tin orbital approach in the atomic sphere approximation (SGF-

TB-LMTO-ASA) [25] using the density functional theory (DFT) [26] in the spin polarization case with the local spin density approximation (LSDA) [27]. The local exchange–correlation potential of the Vosk–Wilk–Nusair parameterization was used [28], and the valence basis consisted of s, p, d and f orbitals. For disordered systems, the potentials were determined self-consistently using the coherent potential approximation (CPA), which is a specific method for the configurational averaging of physical observables related to substitutionally random systems, which simplified such averages by expressing them in terms of the Green function [25].

The IEC is calculated in terms of the difference in total energy of the system in the two magnetic configurations: ferromagnetic (F) and antiferromagnetic (AF) coupled magnetic slabs $J(n) = E_{\mathrm{F}}(n) - E_{\mathrm{AF}}(n)$, where n is the thickness of the spacer layer. To leading order, we can define the IEC aerial energy density E_{iec}, which describes the possible magnetic configuration [29] as:

$$E_{\mathrm{iec}} = -J_1 \frac{\overrightarrow{M_1}\overrightarrow{M_2}}{|\overrightarrow{M_1}||\overrightarrow{M_1}|} - J_2 \left(\frac{\overrightarrow{M_1}\overrightarrow{M_2}}{|\overrightarrow{M_1}||\overrightarrow{M_1}|} \right)^2 = -J_1 \cos(\Delta\varphi) - J_2 \cos^2(\Delta\varphi).$$

$\Delta\varphi$ is the angle between the magnetizations $\overrightarrow{M_1}$ and $\overrightarrow{M_2}$ of the two magnetic slabs, where J_1 is the bilinear coupling describing the F and AF coupling, which correspond to $\Delta\varphi = 0$ and $\Delta\varphi = \pi$, respectively. J_2 is the biquadratic coupling, which describes the $\frac{\pi}{2}$ coupling. If we neglect J_2, the bilinear coupling J_1 is $J_1 = \frac{-J}{2A}$, where A is the area occupied by the two-dimensional (2D) interface unit cell and J is our working parameter, which takes the inverse sign of the conventional coupling parameter J_1. If $J > 0$, the AF configuration is more favorable and J_1 is negative, in agreement with the conventional definition of the coupling parameter J_1. According to our definition of the energy difference, a positive value favours AF coupling and a negative value favours F coupling.

In our calculations we did not find it necessary to include the effects of strong electronic correlations, spin–orbit coupling, and non-collinearity of intra-atomic magnetization, since we will show later that our calculations using LDA exhibit very good agreement with the experimental results for the systems that were studied. But for precise calculations, for instance, the correlation effects within the d shell are important for the magnetic anisotropy energy, which is a ground-state property of 3d transition metals. These effects are not shown by the LDA but are described by Hubbard-like interactions [30]. The LDA + U and DMFT (dynamical mean field theory) approaches have been used extensively to study the model Hamiltonian of correlated electron systems in the weak, strong, and intermediate coupling regimes. They have been very successful in describing the physics of realistic systems such as transition-metal oxides [31]. Recently, they have been used to predict the easy axis of Ni, which is a transition metal [32]. Therefore, these methods are expected to treat properly the materials with d or f electrons.

The transport properties are evaluated within a Kubo–Landauer approach in the current perpendicular to the plane (CPP) geometry [21, 33]. The conductance C^σ is the sum over all channels associated with a particular wavevector parallel to the plane, $k_\parallel$, and with spin polarization σ, and can be expressed as:

$$C^\sigma = \frac{e^2}{h} \frac{1}{N_\parallel} \sum_{k_\parallel} \mathrm{Tr} \left\{ B_{\mathrm{L}}^\sigma g_{1,N}^{\sigma+} B_{\mathrm{R}}^\sigma g_{N,1}^{\sigma-} \right\}_{k_\parallel}.$$

$\frac{e^2}{h}$ is usually called the quantum conductance unit, and B_{L}^σ (B_{R}^σ) is the anti-hermitian part of the so-called embedding potential describing the influence of the left (right) semi-infinite side on the left (right) side of the active region. $g_{1,N}^{\sigma+}$ ($g_{N,1}^{\sigma-}$) is the off-diagonal retarded (advanced)

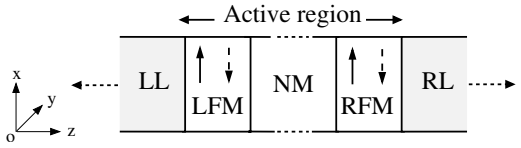

Figure 1. Schematic diagram of the geometry used in the calculation. At the extremities of the figure we have the left lead (LL) and right lead (RL). In the active region we distinguish the left ferromagnetic (LFM) slab and right ferromagnetic (RFM) slab, while in the middle is the non-magnetic (NM) slab. The magnetic moments in the LFM and RFM were in the plane (xoy) and their orientation with respect to each other is taken parallel or antiparallel.

scattering path operator linking the left lead (LL) and right lead (RL). The trace is taken over angular momentum and sites in the principal layer unit cell; all quantities were evaluated at the Fermi energy. For the disordered system the CPA potential parameters obtained from a self-consistent electronic structure calculation were used in the transport calculation. We used the definition of the GMR as the ratio of the difference in the total conductivities in both configurations over the total conductivity in the AF configuration:

$$\mathrm{GMR} = \frac{C_{\mathrm{F}}^{\mathrm{total}} - C_{\mathrm{AF}}^{\mathrm{total}}}{C_{\mathrm{AF}}^{\mathrm{total}}}$$

with

$$C_{\mathrm{F}}^{\mathrm{total}} = C_{\mathrm{F}}^{\uparrow} + C_{\mathrm{F}}^{\downarrow} \qquad F$$
$$C_{\mathrm{AF}}^{\mathrm{total}} = 2C_{\mathrm{AF}}^{\uparrow} = 2C_{\mathrm{AF}}^{\downarrow} \qquad AF.$$

3. Computational details

The geometries of our layered structures, shown in figure 1, were all composed of semi-infinite LLs and RLs sandwiching a trilayer, which is called the active region made, in turn, of a left and a right ferromagnetic slab of a fixed thickness (LFM and RFM) separated by a non-magnetic spacer (NM) of varying thickness. Furthermore, in all our calculations the LL and RL are kept identical physically, and likewise for the LFM and RFM. The procedure for our calculations is described thoroughly in [25], but here we will only describe the major steps involved in our calculations. The atomic calculations were performed as a first step to obtain the potential parameters (PPs), which are collected together for each sample and used as starting parameters for either bulk or active region calculations. Since, in our case, LL and LR are identical for each sample, we only needed to calculate the leads' electronic bulk fundamental state once. At thermodynamical equilibrium the Fermi energy of the whole sample is the same everywhere. As far as the thickness of the active region is negligible compared to the lead's thickness, the Fermi energy of the whole sample may be approximated to the Fermi energy of the lead. Thus, we have taken the Fermi energy of the whole sample as the Fermi energy of the lead. The second step consists of spin-polarized SGF calculations in the active region for the two F and AF phase configurations for each sample. Consequently, the output of the previous run is used to calculate the conductance for each magnetic configuration. In table 1 we show the chemical and structural compositions of the systems studied. The active region was considered as the structural continuity of the leads.

The magnetic slabs in samples C and D are disordered alloys. On the other hand, sample E has magnetic slabs with the same chemical composition as sample D, but the structure consists of an alternation of monoatomic layers of Fe and Pt. The Wigner seitz radius (WSR) is taken in

Table 1. Input structural parameters. Notice that LFM and RFM for samples C and D are disordered, but for sample E it is an alternation of monoatomic planes of Fe and Pt in the growth direction. The cell parameters are taken from [34].

	LL = RL					
				Cell parameters		
Sample	Element	Phase	Growth direction	a (Å)	c/a	Active region LFM/NM/RFM
A	Co	hcp	(0001)	2.505	1.623	Co/Os/Co
B	Fe	bcc	(110)	2.866		Fe/Os/Fe
C	Fe	bcc	(110)	2.840		$Fe_{0.5}Co_{0.5}$/Os/$Fe_{0.5}Co_{0.5}$
D	Pt	fcc	(001)	3.860		$Fe_{0.5}Pt_{0.5}$/Os/$Fe_{0.5}Pt_{0.5}$
E	Pt	fcc	(001)	3.860		FePt/Os/FePt

Table 2. Calculated and experimental lattice parameters for the active magnetic layers. For the lattice parameter, the corresponding WSR in parentheses were deduced by space filling of the unit cell with the atomic spheres.

		Lattice parameter			
		Experimental[a]		Calculated[b]	
Elements	Structure type	a (Å)	c/a	a (Å)	c/a
Co	hcp	2.505(2.61)	1.623	2.468(2.56)	1.605
Fe	bcc	2.866(2.66)		2.795(2.60)	
FeCo	CsCl	2.85(2.64)		2.81(2.61)	
FePt	L10	3.86(2.83)	0.981	3.823(2.78)	0.961

[a] From [34].
[b] By the TB-LMTO Stutgart code.

conjunction with the input structure parameters. The active region is divided into N principal layers (PL) which are indexed by $1 \leqslant p \leqslant N$, while the LL and the RL correspond to $p \leqslant 0$ and $p \geqslant N + 1$, respectively. Here, we only consider the first-nearest-neighbor interaction coupling of PLs via the structure constants, for which their spatial extent is minimized within the TB-LMTO representation β [19]. Meanwhile, in systems with face-centered cubic (fcc) and hexagonal close-packed (hcp) structure, one PL was formed by two neighboring atomic layers in the fcc(001) and hcp(0001) stacking directions, while one atomic layer per PL was sufficient in the body-centered cubic bcc(110) stacking direction [25].

An additional bulk energy optimization for the lattice constant of ferromagnetic materials forming the magnetic slab is performed with the TB-LMTO-ASA Stuttgart code [35] for comparison (see table 2). The corresponding experimental WSRs which we used in Stuttgart code calculations are obtained by space filling of the unit cell with atomic spheres. For Co in the hcp structure and FePt in the $L1_0$ structure, the optimized a and c/a parameters with respect to the total energy were obtained by varying both of them, then the minimized energy is obtained by an energy polynomial fit with respect to the two parameters. For the layered systems for the samples listed in table 1, where we use the SGF-TB-LMTO-ASA-CPA, as coded by Turek and coworkers [25], the total energy was evaluated for the studied system in the F and AF configurations, where surface Brillouin zone (SBZ) integrations were performed on a uniform mesh of 20×20 to 25×25 in $k_{\|}$; the energy contour integrations over the occupied part of the valence bands were performed in the complex energy plane along a whole circle on

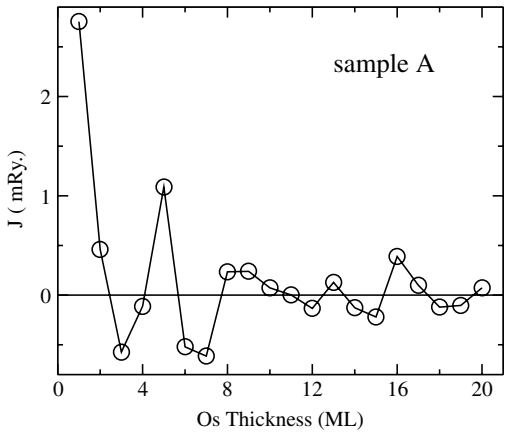

Figure 2. Interlayer exchange coupling in sample A as a function of the number of Os layers n. The solid line connecting the symbols is a guide to the eye in this figure and in all the following figures.

a mesh of 14 points. For the transport calculation in disordered systems we used 40×40 to 100×100 $k_{\|}$ points in the SBZ, and an average conductance over the configurations of the two alloys is evaluated in a 2×2 two-dimensional lateral supercell. For an ordered system, we use 400–800 k-points in the SBZ.

4. Results and discussion

For sample A in table 1 we have calculated the total energy for the F and AF configurations. In figure 2 we show the dependence of J on the Os thickness n. As we can see in this figure, an oscillation between AF and F coupling is clearly present. The AF coupling occurs at 1–2 ML, with a strong peak at 1 ML and 5 ML ($\approx$ 10Å), with a strength smaller than the latter by about a factor of three, then at 8–10 ML ($\approx$16–20 Å), 13 ML ($\approx$26 Å) and 16–17 ML ($\approx$32 Å) with minor peaks. Experimentally, Chou *et al* [6] found that, for AF coupling in the Co/Os/Co trilayer, prepared by a magnetron sputtering technique with an Os spacer thickness of 7–13 Å, the strongest peak was at 9 Å, which corresponds to our 5 ML, and no other AF coupling was observed up to 20 Å. Also, Bloemen *et al* [5] studied the IEC in Co/Os multilayers prepared using the electron-beam evaporation technique with Os thickness varied from 4 to 36 Å. They found that the first AF coupling peak appears at 9 ± 1 Å with a strong coupling strength and a weak second peak at 25 Å (see figure 2 of [5], top panel). This led them to conclude that the IEC oscillates with a period of approximately 15 Å (7 ML). Thus, with regard to the positions of the AF coupling peaks and their relative amplitudes, our calculations showed very good agreement with the results of Bloemen *et al* [5] in the range of spacer thickness taken in this experiment within the experimental error. Due to the weak intensity of the $\approx$8 ML peak, Bloemen *et al* [5] did not evoke it in the text of their paper, but it is clearly present in our theoretical calculations.

The same calculations have been performed for (Fe, FeCo)(110)/Os_n/(Fe, FeCo)(110), samples B and C, respectively. The dependence of the IEC as a function of the interlayer distance n is shown in figure 3. In sample B, there is a clear AF coupling at an Os thickness of 4 ML (about 8 Å). The AF coupling at $n = 1$ is the strongest for this system. But above 5 ML the IEC is weak, therefore no oscillations will be discussed and emphasized in this range.

Experimentally, Chou *et al* [6] found, for an Fe/Os/Fe trilayer, an AF coupling between 9 and 11 Å in the studied Os spacer thickness range of 7 to 20 Å, which is comparable with our

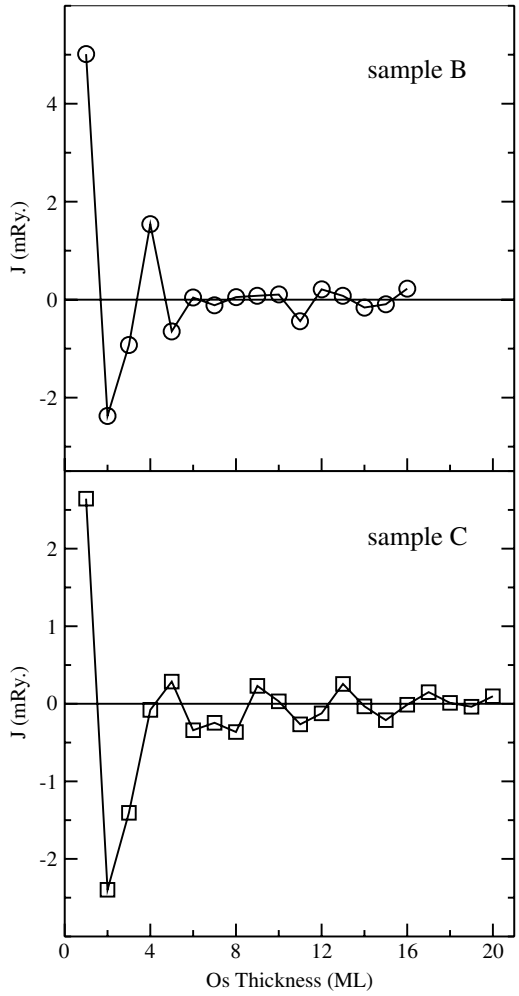

Figure 3. Interlayer exchange coupling as a function of the number of Os layers n for Fe(110)/Os$_n$/Fe(110) (sample B) and FeCo(110)/Os$_n$/FeCo(110) with disordered $Fe_{50}Co_{50}$ alloy (sample C).

results. On the other hand, the effect of Co addition is clearly seen in sample C in figure 3, where an oscillation of roughly 4 ML (8 Å) is obvious to the eye. The AF coupling peaks are located at 1, 5, 9, 13 and 17 ML, respectively, with a damping strength. The same behavior of the IEC for $n = 1$ ML is found as in samples A and B with the strong AF coupling strength. Chen *et al* [7] studied the IEC of an FeCo/Os/FeCo trilayer, prepared by dc magnetron sputtering in the range of Os thickness between 3 and 20 Å, where they found an AF coupling between 7 and 13 Å with a maximum peak at about 9 Å, which is in good agreement with our second peak located at 5 ML (about 10 Å). If we exclude the trivial case of 1 ML AF IEC, we notice that the first AF IEC appeared at 4 ML for sample B and at 5 ML for sample C. This lag of 1 ML might be explained qualitatively by the phase shift [36] induced by the electronic properties of the ferromagnetic materials.

For samples D and E, the dependence of the IEC with n is shown in figures 4(a) and (c), respectively. On the one hand, the IEC for both samples oscillates rapidly with a period of

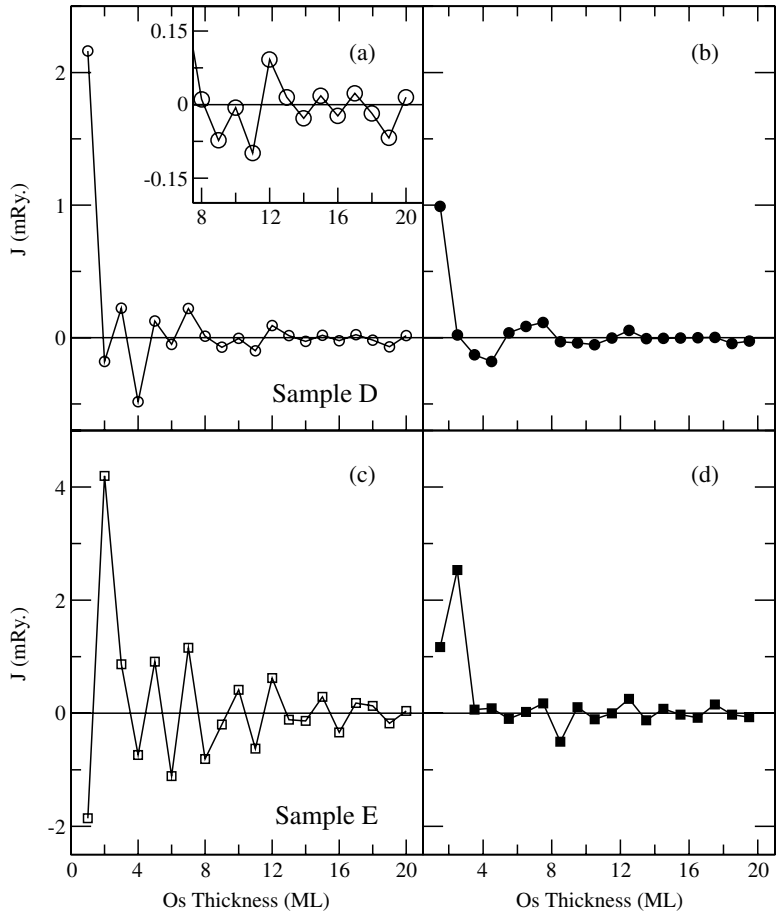

Figure 4. Interlayer exchange coupling as a function of the number of Os layers n for FePt(001)/Os_n /FePt(001) with disordered $Fe_{0.50}Pt_{0.50}$ alloy (sample D (a)) and ordered FePt alloy in $L1_0$ structure (sample E (c)). The introduction of the possible surface roughness effect is as in [37] for the two samples, shown in the right-hand panels (b) and (d). The inset in (a) shows the change in the coupling from AF–F to F–AF oscillation and vice versa every 5 ML.

approximately 2 ML, and on the other hand the coupling is changing from AF–F to F–AF oscillation and vice versa. For instance, in sample D changes occur at 8, 13 and 18 ML i.e. every 5 ML; we will discuss this point later within the Ruderman–Kittel–Kasuya–Yosida (RKKY) model. For a very thin spacer, i.e. $n = 1$ and 2 ML, the phase of the coupling is reversed in sample E compared to sample D and hence the first AF coupling peak is shifted to 2 ML. It is obvious from the scales in this figure that the amplitudes of the couplings in sample E are greater than those in sample D, therefore the ordering alloy of the ferromagnetic slab enhances the coupling strength of the disordered alloy slab. It is argued that, due to surface roughness, the short period oscillations are hard to detect experimentally. We choose a simple model to introduce the effect of roughness of the interfaces on the IEC period. In figures 4(b) and (d) we show the calculated average value of J between subsequent layers of Os spacer via equation (1).

$$\left\langle J\left(n+\tfrac{1}{2}\right)\right\rangle = \tfrac{1}{2}\left[J(n)+J(n+1)\right] \tag{1}$$

Table 3. Fitted parameters via equation (2).

Sample	i	A_i (mRyd)	T_i (ML)	φ_i (rad.)	χ^2
A	0	2.0	2.9	−2.2	0.010
	1	12.3	6.8	−0.9	
	2	26.5	3.7	−7.2	
B	0	1.3	2.1	3.5	0.002
	1	22.7	3.9	−5.6	
	2	26.3	3.1	−5.2	
C	0	5.4	3.5	4.2	0.013
	1	34.2	4.1	0.3	
	2	59.8	3.5	−5.1	
D	0	0.3	2.8	6.5	0.001
	1	7.7	2.5	−4.5	
	2	6.2	5.5	0.1	
E	0	4.6	2.7	−1.9	0.009
	1	32.1	2.4	1.4	
	2	7.5	5.5	0.7	

which corresponds to a possible surface roughness effect [37]. In figure 4(b), we can see that the short-period oscillation of the IEC is suppressed and a long-period oscillation appears with about 5.5 ML (11 Å), where the strength of the coupling vanishes for $n > 12$ ML. In figure 4(d), only one strong peak with AF coupling still exists at ≈2 ML, while there is no obvious long-period oscillation.

Chen *et al* [8] studied the IEC in a FePt/Os/FePt trilayer prepared by dc magnetron sputtering in the range of Os spacer thickness between 0 and 9 Å, where the FePt alloy has a disordered structure; they found only an AF coupling between 1 and 3 Å, with a maximum strength at 2 Å. This result is in very good agreement with our calculated result, especially when we introduce the effect of the interface roughness; we found that the second region where the AF coupling occurred is at 5–8 ML (≈11–16 Å), which is outside the varied range of the Os thickness considered in the experimental work of Chen *et al* [8].

As we have shown in figures 2–4, discussed qualitatively up to now, the exchange coupling as a function of the Os layer presented damped oscillation behavior for all samples. This will lead us to the well-known RKKY theory to quantify our discussion. In this theory, the asymptotic limit exchange coupling may be modelled by the following function [38]:

$$J(n) = \frac{A_0}{n} \sin\left(\frac{2\pi n}{T_0} + \varphi_0\right) + \sum_{i=1}^{2} \frac{A_i}{n^2} \sin\left(\frac{2\pi n}{T_i} + \varphi_i\right) \tag{2}$$

where n is the spacer thickness, A is the amplitude of the coupling, T is the period and φ is the phase. The pre-asymptotic terms are cancelled out by taking n, i.e. the thickness of the spacer, to be larger than 4 ML. The term which has $1/n$ dependence is for full planar nesting, which describes the short-period oscillation, whereas the second term, which has $1/n^2$ dependence, is the asymptotic limit for larger thicknesses of spacer describing the usual RKKY-type interaction, i.e. $n \to \infty$ [39].

We have fitted the data for our calculations to equation (2) and the fitting parameters are summarized in table 3. The fitted function to the third order for sample A shows the presence of a period of 3.7 ML, which corresponds to the 4 ML oscillation discussed in figure 2, as well as a longer period of 6.8 ML which is close to the measured value of (7 ML) reported by Bloemen *et al* [5], and finally the shortest period corresponds to the smallest signal strength where $A_0/A_1 = 0.16$ and $A_0/A_2 = 0.08$.

In figure 3 for sample B, the curve shows strong damping after the pre-asymptotic region. The obtained results show a short period of 2 ML with small strength and two long periods with very close strengths of 3.1 and 3.9 ML.

For sample C the oscillation periods obtained are within the range of the values predicted by Stiles [9] if we consider the (1100) hcp interface as a (110) bcc-like interface.

Our fit parameters for samples D and E, if we assume that (1120) hcp and (001) fcc interfaces are closely equivalent, are in good agreement with the periods reported by Stiles [9]. The long period of ≈5.5 ML is clearly seen in figure 4(b) by introducing an artificial surface roughness effect type, via equation (1). The two short periods extracted for sample D (E) are close to each other, 2.8 (2.7) and 2.5 (2.4), where the period of 2.5 (2.4) has dominant strength, and they lead to a beat phenomenon seen in figures 4(a) and (c).

We have to point out that the modified forms of the RKKY method relate the IEC period to wavevectors in the Fermi surface. These models are based on the different topological forms of the Fermi surface. So far, a naive spherical Fermi surface [40]—a calculated Fermi surface using LDA or fits of Fermi surface data obtained from de Haas–van Alphen and cyclotron-resonance experiments of the spacer layer—have been used besides the moment distribution within the ferromagnetic layers [41, 42]. As far as we are concerned, work is underway to find the relationship between the wavevectors and our periods for the whole systems cited above, and this will published on separate paper.

Figure 5 shows the partial conductance (left-hand panels) and GMR (right-hand panels) for the samples studied. Oscillations of the IEC are seen in the GMR. More precisely, the conductivity of spin-up electrons in the F configuration ($C_{\mathrm{F}}^{\uparrow}$) reflect very well the oscillation behavior of IEC in samples A, B, and C. Also, in samples D and E the period oscillation of 2 ML is seen clearly in the conductance of spin-down electrons in the F configuration, $C_{\mathrm{F}}^{\downarrow}$, more than in $C_{\mathrm{F}}^{\uparrow}$. Meanwhile, the conductance in the AF configuration, C_{AF}, in most samples shows a thickness independence for thicknesses greater than 4 ML, except for sample D where they oscillate as $C_{\mathrm{F}}^{\downarrow}$. The increase in C_{AF} caused a decrease in GMR, seen in a disordered alloy in magnetic slabs (sample C and D). Comparing samples D and E, the increase in the overall conductance due to disorder is not fully compensated by their spin asymmetry, which gives rise to a decrease in the GMR with respect to the ordering alloy. The ordering of a magnetic slab enhances the GMR ratio.

The conductance of the two systems, a Co/Os/Co trilayer (sample A) and an Fe/Os/Fe trilayer (sample B), compared to the same systems but with a Cu or Cr spacer layer ($C_{\mathrm{F}}^{\uparrow}$ and $C_{\mathrm{F}}^{\downarrow}$ in the F configuration) are inverted [43]. In contrast, in Co/Os (Co/Cu), $C_{\mathrm{F}}^{\downarrow}$ has a greater (smaller) component and $C_{\mathrm{F}}^{\uparrow}$ has a smaller (greater) component, and in Fe/Os (Fe/Cr) $C_{\mathrm{F}}^{\uparrow}$ has a greater (smaller) component and $C_{\mathrm{F}}^{\downarrow}$ has a smaller (greater) component. To illustrate this behavior, let us first take a look at the magnetic and electronic structure of the two samples. Figure 6 shows the profiling of the magnetic moment across samples A and B in the AF configuration. Os in both cases showed a null total magnetization and a magnetic moment distribution characterizing a spin-wave-like motion. The magnetic moment of the Co of the first atomic layer from the interface is reduced. This is not the case for Fe, where no noticeable variation was observed. Furthermore, the coupling of the magnetic moment at the interface is ferromagnetic type for Fe/Os and ferrimagnetic type for Co/Os. No magnetic dead layer was observed at the interface, as suggested by [5]. The results for the magnetic moment are, to some extent, independent of the Os spacer layer thickness. The density of states of Os atoms is composed of an almost d-component at the Fermi energy for both spins. So, the current at the Fermi energy level has a strong d-character in the spacer layers, while in the magnetic slabs only the electrons with spin down for Co and spin up for Fe have a strong d-character and can

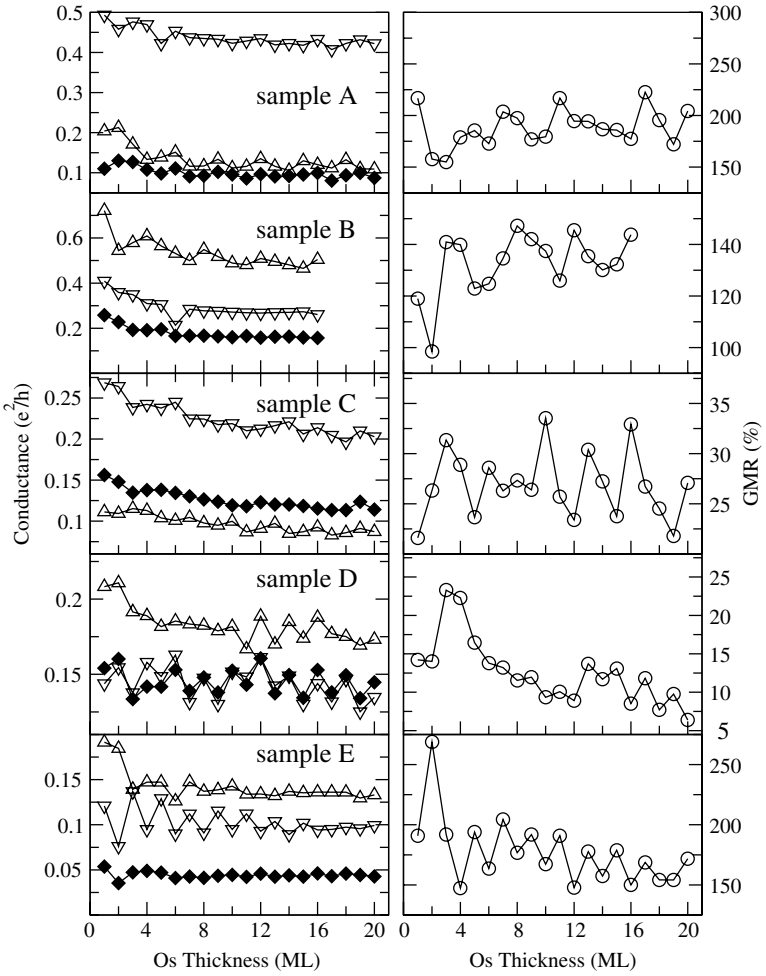

Figure 5. Conductance (left) and GMR (right) for all samples as a function of the number of spacer layers n. In the left-hand panel the (open) up triangle represents $C_{\mathrm{F}}^{\uparrow}$, the (open) down triangle represents $C_{\mathrm{F}}^{\downarrow}$ and the (closed) diamond represents C_{AF}. In the right-hand panels the open circle represents the GMR ratio.

move easily through the spacer, while those electrons with spin up in Co and spin down in Fe are a mixture of s-, p-and d-character, which cause scattering at the interfaces, inter-band scattering, and hence reduce the conductance for these channels [44, 45].

5. Conclusion

We have studied the IEC oscillation and the transport properties for a series of ferromagnetic layers sandwiching an Os non-magnetic spacer with varying thickness, using a self-consistent surface Green's function technique based on the tight-binding linear muffin-tin orbital method in the atomic sphere approximation. The coherent potential approximation was used to describe the alloying.

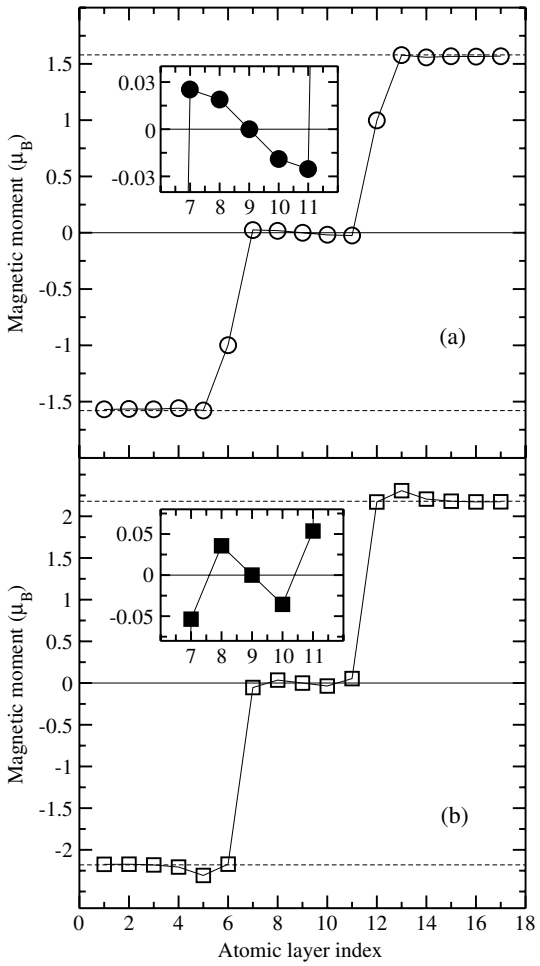

Figure 6. Magnetic moment profile in the AF configuration for sample A (a) and for sample B (b). Here we fix the number of Os layers to 5 ML and the number of LFM and RFM layers to 6 ML. The insets show the profile of Os. The vertical dashed lines denote the bulk magnetic moments for Co and Fe in (a) and (b), respectively.

The mostly AF coupling peak observed experimentally for an Os spacer thickness of 9–10 Å and for each ferromagnetic slab used (Fe, Co and FeCo) matches our calculated results very well. For FePt/Os/FePt, we have attributed the AF coupling peak observed experimentally at an Os spacer thickness of 1 ML to our calculated AF coupling at 1 ML in a disordered magnetic layer. By introducing the effect of the interface roughness in our calculations, we found that the peak is shifted towards 1.5 ML. We fitted our IEC results to a RKKY function to the third order to obtain quantitatively the periods of oscillations and their strengths. In the Co/Os/Co system we have found that the values of the oscillation periods of the IEC are 4 ML, which was not observed experimentally, and 7 ML, which was observed experimentally. Unfortunately, the lack of experimental data for the periods of oscillations in FeCo/Os/FeCo, Fe/Os/Fe and FePt/Os/FePt did not allow us to compare our results presented above. However, our results in these systems are in good agreement with another calculation method [9].

For the transport properties we found that the main effect controlling magnetic transport in the case of an Os spacer layer was inter-band scattering. An enhancement in GMR of about 180% is observed for an ordered ferromagnetic slab for FePt compared to a FePt/Os/FePt trilayer with a disordered ferromagnetic slab, for which the enhancement is about 15%.

Acknowledgments

We are in debt to M Alouani's group for providing us with the code SGF-TBLMTO-ASA-CPA, and specially to O Bengone for fruitful discussions. We thank M Kharoubi for previous collaboration. We thank the support of eJDS International Centre for Theoretical Physics-Science Dissemination Unit for providing us with the necessary references.

References

[1] van den Berg H A M, Coehoorn R, Gijs M A M, Grünberg P, Rasing T and Röll K 2006 *Magnetic Multilayers and Giant Magnetoresistance: Fundamentals and Industrial Applications* ed U Hartmann (New York: Springer)
[2] Mills D L and Bland J A C 2006 *Nanomagnetism Ultrathin Films, Multilayers and Nanostructures* (Amsterdam: Elsevier)
[3] Grünberg P, Schreiber R, Pang Y, Brodsky M B and Sowers H 1986 *Phys. Rev. Lett.* **57** 2442
[4] Grünberg P, Bürgler D E, Dassow H, Rata A D and Schneider C M 2007 *Acta Mater.* **55** 1171
[5] Bloemen P J H, Jonge W J M and Coehoorn R 1993 *J. Magn. Magn. Mater.* **121** 306
[6] Chou C Y, Yao Y D, Kuo P C, Lee S F and Chou J 2006 *J. Magn. Magn. Mater.* **304** e349
[7] Chen S Y, Yao Y D and Wu J M 2006 *J. Magn. Magn. Mater.* **304** e37
[8] Chen S Y, Yao Y D and Wu J M 2007 *J. Magn. Magn. Mater.* **310** 1914
[9] Stiles M D 1993 *Phys. Rev.* B **48** 7238
[10] Peng T Y, Lo C K, Chen S Y and Yao Y D 2006 *J. Magn. Magn. Mater.* **304** e50
[11] Peng T Y, Lo C K, Chen S Y and Yao Y D 2006 *J. Appl. Phys.* **99** 08C907
[12] Parkin S S P 1991 *Phys. Rev. Lett.* **67** 3598
[13] Stiles M D 1999 *J. Magn. Magn. Mater.* **200** 322
[14] Fishman R S 2001 *J. Phys.: Condens. Matter* **13** R235
[15] Zabel H 1999 *J. Phys.: Condens. Matter* **11** 9303
[16] Pierce D T, Unguris J, Celotta R J and Stiles M D 1999 *J. Magn. Magn. Mater.* **200** 290
[17] Stoeffler D, Ounadjela K and Cautier F 1991 *J. Magn. Magn. Mater.* **93** 386
[18] Stoeffler D C A 1997 *J. Magn. Magn. Mater.* **165** 62
[19] Turek I, Kudrnovsky J and Drchal V 1999 *Lecture Notes Phys.* **535** 349
[20] Kudrnovsky J, Drchal V, Turek I, Bruno P, Dederichs P and Weinberger P 1999 *Lecture Notes Phys.* **535** 313
[21] Kudrnovsky J, Drchal V, Blaas C, Wienberger P, Turek I and Bruno P 2000 *Phys. Rev.* B **62** 15084
[22] Skubic B, Holmström E, Iusan D, Bengone O, Eriksson O, Brucas R, Hjörvarsson B, Stanciu V and Nordblad P 2006 *Phys. Rev. Lett.* **96** 057205
[23] Iusan D, Alouani M, Bengone O and Eriksson O 2007 *Phys. Rev.* B **75** 024412
[24] Drchal V, Kudrnovsky J, Bruno P, Dederichs P H, Turek I and Wienberger P 2002 *Phys. Rev.* B **65** 214414
[25] Turek I, Drchal V, Kudrnovsky J, Sob M and Wienberger P 1997 *Electronic Structure of Disordered Alloys, Surface and Interfaces* (Dordrecht: Kluwer)
[26] Hohenberg P and Kohn W 1964 *Phys. Rev.* **136** B864
[27] von Barth U and Hedin L 1972 *J. Phys. C: Solid State Phys.* **5** 1629
[28] Vosko S H, Wilk L and Nusair M 1980 *Can. J. Phys.* **58** 1200
[29] Borgler D E, Gronberg P, Demokritov S O and Johnson M T 2001 *Handbook of Magnetic Materials* vol 13, p 1
[30] For a review, see, e.g. Anisimov V I (ed) 2000 *Strong Correlations in Electronic Structure Calculations* (New York: Gordon and Breach)
[31] Georges A, Kotliar G, Krauth W and Rozenberg M J 1996 *Rev. Mod. Phys.* **68** 13
[32] Yang I, Savrasov S Y and Kotliar G 2001 *Phys. Rev. Lett.* **87** 216405
[33] Bengone O, Eriksson O, Mirbt S, Turek I, Kudrnovsky J and Drchal V 2004 *Phys. Rev.* B **69** 092406
[34] Brandes E A and Brook G B 1992 *Smithells Metals Reference Book* (London: Butterworth Heinemann)
[35] Krier G, Jepsen O K, Burkhardt A and Andersen O K 2000 *TB-LMTO-ASA* version 4.7 Stutgart, Germany

[36] Johnson M T, van de Vorst M T H, Bloemen P J H, Coehoorn R, Reinders A, aan de Stegge J and Jungblut R 1995 *Phys. Rev. Lett.* **75** 4686
[37] Mirbt S, Skriver H L, Aldén M and Johansson B 1993 *Solid State Commun.* **88** 331
[38] Mirbt S, Niklasson A M N, Johansson B and Skriver H L 1996 *Phys. Rev.* B **54** 6382
[39] Bruno P and Chappert C 1992 *Phys. Rev.* B **46** 261
[40] Baltensperger W and Helman J S 1990 *Appl. Phys. Lett.* **57** 2954
[41] Bruno P and Chappert C 1991 *Phys. Rev. Lett.* **67** 1602
[42] Bruno P 1995 *Phys. Rev.* B **52** 411
[43] Tsymbal E Yu and Pettifort D G 1996 *Phys. Rev.* B **54** 15314
[44] Sanvito S, Lambert C J and Jefferson J H 1999 *J. Magn. Magn. Mater.* **203** 105
[45] Sanvito S, Lambert C J and Jefferson J H 1999 *J. Magn. Magn. Mater.* **196/197** 101